Dynamics of intermediate-mass black holes wandering in the milky way galaxy using the illustris TNG50 simulation

Emma Jane Weller,[1]★ Fabio Pacucci ®,[1,2]★ Lars Hernquist[1] and Sownak Bose ®[1,3]

[1]*Center for Astrophysics | Harvard & Smithsonian, Cambridge, MA 02138, USA*
[2]*Black Hole Initiative, Harvard University, Cambridge, MA 02138, USA*
[3]*Institute for Computational Cosmology, Durham University, South Road, DH1 3LE Durham, UK*

ABSTRACT

The detection of Intermediate-Mass Black Holes (IMBHs) in dwarf galaxies is crucial to closing the gap in the wide mass distribution of black holes ($\sim 3\,\mathrm{M_\odot}$ to $\sim 5 \times 10^{10}\,\mathrm{M_\odot}$). IMBHs originally located at the centre of dwarfs that later collide with the Milky Way (MW) could be wandering, undetected, in our Galaxy. We used TNG50, the highest resolution run of the IllustrisTNG project, to study the kinematics and dynamics of star clusters, in the appropriate mass range, acting as IMBH proxies in an MW analogue galaxy. We showed that ~ 87 per cent of our studied IMBHs drift inward. The radial velocity of these sinking IMBHs has a median magnitude of $\sim 0.44\,\mathrm{ckpc\,h^{-1}\,Gyr^{-1}}$ and no dependence on the black hole mass. The central $1\,\mathrm{ckpc\,h^{-1}}$ has the highest number density of IMBHs in the galaxy. A physical toy model with linear drag forces was developed to explain the orbital circularization with time. These findings constrain the spatial distribution of IMBHs, suggesting that future searches should focus on the central regions of the Galaxy. Additionally, we found that the 3D velocity distribution of IMBHs with respect to the galactic centre has a mean of $\sim 180\,\mathrm{km\,s^{-1}}$ and larger variance with decreasing radius. Remarkably, the velocity distribution relative to the local gas shows significantly lower values, with a mean of $\sim 88\,\mathrm{km\,s^{-1}}$. These results are instrumental for predicting the accretion and radiation properties of IMBHs, facilitating their detection with future surveys.

Key words: black hole physics – methods: numerical – Galaxy: general – Galaxy: kinematics and dynamics.

1 INTRODUCTION

Black holes cover a wide range in mass and have been detected over a very large fraction of the known Universe. Stretching from $\sim 3\,\mathrm{M_\odot}$ (Thompson et al. 2019) to $\sim 5 \times 10^{10}\,\mathrm{M_\odot}$ (Dullo, Gil de Paz & Knapen 2021), they have been identified as close as $\sim 1000\,\mathrm{pc}$ (Oke 1977) and as far as $z = 7.642$ (Wang et al. 2021).

Two populations of black holes have been broadly investigated and located in specific environments. Stellar-mass black holes, with typical mass $\lesssim 10^3\,\mathrm{M_\odot}$, are ubiquitous in the volume of galaxies. According to recent estimates (e.g. Elbert, Bullock & Kaplinghat 2018), the Milky Way (MW) may host $\sim 10^8$ such black holes in its volume. Supermassive black holes (SMBHs), with masses $\gtrsim 10^6\,\mathrm{M_\odot}$, are typically found at the centre of massive galaxies. The MW hosts an SMBH of $\sim 4 \times 10^6\,\mathrm{M_\odot}$ (e.g. Ghez et al. 2008; Genzel, Eisenhauer & Gillessen 2010), and the near-horizon features of the central object in M87 were recently imaged by the EHT collaboration in a landmark result (Event Horizon Telescope Collaboration 2019).

Profound correlations exist between the mass of the central black hole and some properties of the host galaxy, such as its stellar mass and velocity dispersion (Ferrarese & Merritt 2000; Gebhardt et al. 2000), suggesting a co-evolution between the massive central object and the host (Kormendy & Ho 2013). Extending these correlations to smaller black hole masses, it is reasonable to expect that black holes

in an intermediate-mass range ($10^3\,\mathrm{M_\odot} \lesssim M_\bullet \lesssim 10^6\,\mathrm{M_\odot}$), known as intermediate-mass black holes (IMBHs), should be contained in dwarf galaxies (see e.g. the recent review by Greene, Strader & Ho 2020). It is unclear whether these correlations hold down to very low masses, or break down instead (see e.g. Baldassare et al. 2017; Pacucci et al. 2018; Nguyen et al. 2019; Baldassare et al. 2020 for different perspectives on the topic). However, clear detections of IMBHs as light as $5 \times 10^4\,\mathrm{M_\odot}$ are reported in dwarf galaxies (Baldassare et al. 2015), and a sizable fraction of their nuclei are predicted to be active (Pacucci, Mezcua & Regan 2021), i.e. hosting accreting black holes.

The MW Galaxy has experienced numerous mergers during its cosmic history, which have possibly inserted IMBHs within its volume. Recent studies suggest that the MW has experienced 15 ± 3 mergers with galaxies with stellar masses $\gtrsim 4.5 \times 10^6\,\mathrm{M_\odot}$ (Kruijssen et al. 2020). These captured IMBHs could still be wandering inside the MW, with low-level accretion that makes them very challenging to detect. The investigation of these wandering and undetected IMBHs is fairly recent (see e.g. Bellovary et al. 2010; González & Guzmán 2018; Greene et al. 2021; Ricarte et al. 2021a,b). In particular, Ricarte et al. (2021b) suggest that thousands of wandering black holes, also of supermassive size, might be found inside galaxy cluster haloes.

In order to guide future observational efforts to detect IMBHs wandering in the MW, it is instrumental to understand their dynamics and kinematics. Where are IMBHs most likely located in the MW Galaxy, and what is their typical velocity? Furthermore, which forces act on them, and what is their typical sinking time? In this study, we

★ E-mail: emmaweller@college.harvard.edu (EJW);
fabio.pacucci@cfa.harvard.edu (FP)

use the TNG50 volume of the IllustrisTNG project (Nelson et al. 2019a) to provide some answers to these questions.

It is important to remark that in this paper we focus only on IMBHs formed in dwarf galaxies and captured by the MW. Of course, other formation processes for IMBHs have been proposed, including: (i) runaway mergers in globular star clusters (e.g. Portegies Zwart & McMillan 2002; Gürkan, Freitag & Rasio 2004; González et al. 2021; Shi, Grudić & Hopkins 2021), (ii) hyper-Eddington accretion on to stellar-mass black holes (e.g. Ryu et al. 2016), (iii) direct collapse of hypermassive quasi-stars (e.g. Volonteri & Begelman 2010; Schleicher et al. 2013), and (iv) supra-exponential accretion on seed black holes (e.g. Alexander & Natarajan 2014; Natarajan 2021). Each of these channels would produce a different number density of IMBHs, as well as different spatial distributions, with likely very different dynamical properties. For example, IMBHs formed *in-situ* would probably have a lower typical velocity with respect to the local gas and stars. It is thus important to keep in mind that in this study we are focusing only on a specific formation channel for IMBHs.

We use the Planck Collaboration VI (2020) cosmology as a reference. In the following Section 2 we describe the simulation suite used, as well as our method to select IMBH proxies. In Section 3 we describe the location of IMBHs in the MW and the radial evolution of their orbits, while in Section 4 we study their kinematics, regarding 3D and radial velocities, and dynamics. Finally, in Section 5 we discuss the conclusions of our work.

2 SIMULATION

In this section, we present the simulation suite and the methodology used to select IMBH proxies, as well as the MW analogue galaxy.

2.1 TNG50

IllustrisTNG (Marinacci et al. 2018; Naiman et al. 2018; Nelson et al. 2018; Pillepich et al. 2018a,b; Springel et al. 2018; Nelson et al. 2019a) is a suite of cosmological simulations performed with the moving-mesh code AREPO (Springel 2010). Each simulation solves the evolutionary equations for dark matter, gas, stars, and SMBHs in a self-consistent fashion, from $z = 127$ to $z = 0$ (Nelson et al. 2019a). For the purpose of this study, we used TNG50-1 (Nelson et al. 2019b; Pillepich et al. 2019), which is the simulation with the highest resolution. TNG50-1 has 2×2160^3 resolution elements, a volume of 35^3 cMpc^3 h^{-3} (or $\sim 50^3$ cMpc^3, hence the name), and a mean time of ~ 0.138 Gyr between snapshots. TNG50-1 also has three sub-boxes, defined as volumes of the simulation with data saved at a higher time cadence (Nelson et al. 2019b).

At $z = 0$, the collision-less components (including star objects, which we use as IMBH proxies – see Section 2.2) have a gravitational softening length of 288 pc (Nelson et al. 2019b). This is smaller than the scales on which we study black hole dynamics ($\gtrsim 1$ kpc), so the relevant gravitational interactions are not affected.

In TNG50 the baryon and dark matter particle masses are 8.5×10^4 M$_\odot$ and 4.5×10^5 M$_\odot$, respectively. Since our IMBH proxies have a mass range of $\sim (2.6 - 9.9) \times 10^4$ M$_\odot$, this might suggest that the dynamical friction is possibly underestimated in certain situations, which then leads to a slight overestimation in the surviving IMBH population. None the less, the sinking time-scales that we find are ~ 10 Gyr, which is of the order that is expected for these objects under the influence of dynamical friction (Binney & Tremaine 1987).

2.2 Identifying captured IMBH proxies

The black hole objects in the simulation mostly fall in the supermassive range – the least massive black hole object in TNG50-1 at $z = 0$ is $\sim 1.2 \times 10^6$ M$_\odot$, which is larger than the mass range we aim to study. Instead, we used star (cluster) objects between 10^4 and 10^6 M$_\odot$ as IMBH proxies. This is acceptable because we are only interested in gravitational effects on large scales. We used two methods to select IMBHs captured by the MW, which we describe in turn.

In the first, we used a list of $z = 0$ MW and M31 analogue galaxies in the simulation (Engler et al. 2021; Pillepich et al. 2021). We identified a total of four MW analogues whose centres of mass fall within one of the three TNG50-1 sub-boxes at snapshot 99 ($z \approx 0$). We then searched the merger trees of these MW analogues for dwarf galaxies, defined as subhaloes in the mass range $10^6 - 10^{10}$ M$_\odot$. We limited the search to more recent mergers, considering only dwarfs that appear after snapshot 60 (~ 7.4 Gyr) in the merger tree. We selected IMBH proxies from these dwarfs that end up in the corresponding MW analogue (and within the sub-box) by $z = 0$. We focused on IMBHs centrally located in their host dwarfs, so we required the IMBHs to be less than 0.01 ckpc from the dwarf centre-of-mass (at the snapshot in which the dwarf appears in the MW analogue merger tree). A total of four IMBHs, with masses in the range $\sim (3.4 - 8.5) \times 10^4$ M$_\odot$, met all the abovementioned conditions. We call this group Set 1. Extending the distance limit from the dwarf centre-of-mass to 0.05 ckpc, we obtained 385 captured IMBH proxies, with masses between $\sim (3.0 - 9.1) \times 10^4$ M$_\odot$. We call this group Set 2, and we use it to have a richer statistical population. All of the IMBH proxies in Sets 1 and 2 turned out to come from the same dwarf galaxy (Subhalo ID 456591 at snapshot 71, or ~ 9.2 Gyr) and end up in the same MW analogue (Subhalo ID 565089 at snapshot 99). This MW analogue falls within sub-box 2, which contains 0.3 per cent of the full simulation volume and has a mean time of ~ 0.004 Gyr between snapshots. We did not find a satisfactory explanation for why all of the suitable IMBHs came from the same dwarf, although it is important to note we only considered dwarfs that merged recently with just four MW analogues, so our collection was small to begin with.

To obtain a larger and more varied set of IMBHs for a larger statistical sample, we developed a second selection method. Rather than use the sub-boxes, we returned to the main simulation, but kept the same MW analogue (Subhalo 565089) for consistency. We tested every 20th IMBH proxy in the galaxy at snapshot 99 ($z \approx 0$) and selected each one that, at the first snapshot after its birth, was not in the main progenitor of the MW analogue. This resulted in 2148 captured IMBH proxies, with masses between $\sim (2.6 - 9.9) \times 10^4$ M$_\odot$, which we call Set 3. We find that the IMBHs in this set enter the MW over a period of 88 snapshots (~ 13.0 Gyr).

It is important to note that the mass range covered by our three sets is only ~ 7.4 per cent of the mass range we canonically assigned to IMBHs (10^4 to 10^6 M$_\odot$). This makes sense, as the largest star cluster object in the MW analogue 565089 at $z = 0$ is just 1.4×10^5 M$_\odot$. This limited mass range is not ideal, but we believe it is better than using the black hole objects, which are far too large.

A summary of the characteristics of the three sets is given in Table 1. Two additional sets, both subsets of Set 3, are also included in the table, and described in Section 3.2.

Each star cluster acting as an IMBH proxy is tracked by its particle ID, which remains constant throughout the simulation. Single stars within a cluster cannot be tracked, because they do not possess individual identifiers in the Illustris TNG50 simulation. In order to track the position of IMBH proxies throughout the simulation, for each snapshot of interest an array of particle IDs of star cluster

Table 1. Summary features of the five IMBHs sets employed.

Set #	IMBHs contained	Selection criteria for IMBH set
1	4	Distance <0.01 ckpc from dwarf centre; obtained from sub-boxes
2	385	Distance <0.05 ckpc from dwarf centre; obtained from sub-boxes
3	2148	Captured IMBHs that originate outside MW analogue; obtained from main simulation
4	953	Subset of Set 3 that meets certain conditions described in Section 3.2
5	825	Sinking IMBHs from Set 4

objects in the given MW analogue was retrieved, along with arrays containing the particle properties of relevance. The properties of a given IMBH proxy were then found by locating the star cluster's particle ID against the full list of particle IDs.

2.3 MW analogue galaxy

As explained in Section 2.2, although there are many MW and M31-like galaxies in TNG50, only four lie in the sub-boxes, and our analysis uses just one of them – namely Subhalo 565089. This was the only galaxy containing IMBHs that met the strict constraints for Sets 1 and 2. Thus, when we needed to loosen our selection criteria for Set 3 to obtain a larger number of IMBHs, focusing on IMBHs from Subhalo 565089 seemed like a natural choice. This also adds consistency across Sets 1–3, making results from the different sets more comparable. This is quite valuable, as we switch between the sets frequently throughout our study.

In the following sections, we will refer to Subhalo 565089 as 'the MW analogue' or simply 'the MW'. Additionally, the subhalo centre-of-mass property is not available in the sub-boxes, hence we use the subhalo position for all relative motion calculations. Thus, 'MW centre' refers to the position of Subhalo 565089.

3 LOCATION AND RADIAL EVOLUTION OF INTERMEDIATE-MASS BLACK HOLES

In this section, we describe the location of IMBHs in the MW, as well as their tendency to sink towards the centre of the galaxy.

3.1 Time evolution of radial distance

For each IMBH in Set 1, we calculated the x, y, and z coordinates relative to the MW centre at every sub-box snapshot from present time back to the time when the IMBH first entered the sub-box. These orbits are shown, for illustration purposes, in Fig. 1. These IMBHs have masses in the range $(3.4 - 8.5) \times 10^4 \, M_\odot$ and various orbital distances from the MW centre.

We then used these data to calculate the distance from the MW centre at each snapshot for each IMBH in Set 1. Binning the distances to reveal overall trends, we obtained the results shown in Fig. 2. We repeated the same process for Set 2, but rather than binning the distances, we only calculated the distance at every 20th sub-box snapshot, for computational simplicity. The results are shown in Fig. 3, where the central solid line is the median, while the shaded range indicates dispersion via the interquartile range.

Figs 2 and 3 indicate that the radial distances of IMBHs tend to decrease with increasing time. This fits with our expectation that captured IMBHs sink towards the galactic centre, an effect that is explained by mass migration due to dynamical friction. Earlier works have already suggested that black holes, which are among the heaviest objects in galaxies, tend to cluster in the galactic centre over time. For example, Miralda-Escudé & Gould (2000) suggested
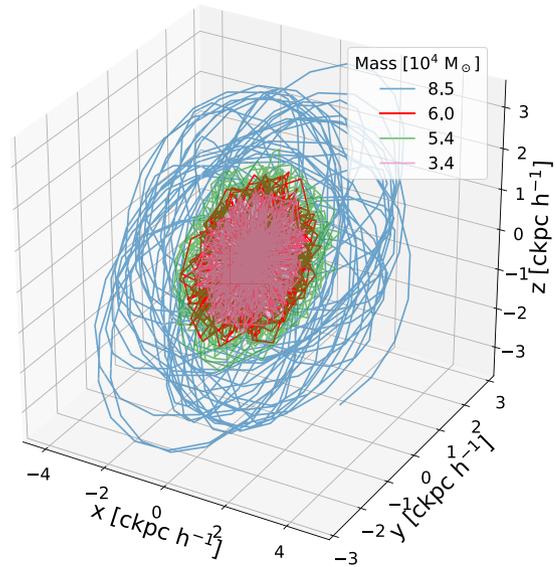
Figure 1. 3D orbits of IMBHs in Set 1 for illustration purposes. These IMBHs originate in a dwarf galaxy, within 0.01 ckpc of the centre. The position of the IMBH is calculated with respect to the position of the MW centre at every sub-box snapshot over a mean time period of ~571 snapshots (~ 4.42 Gyr).
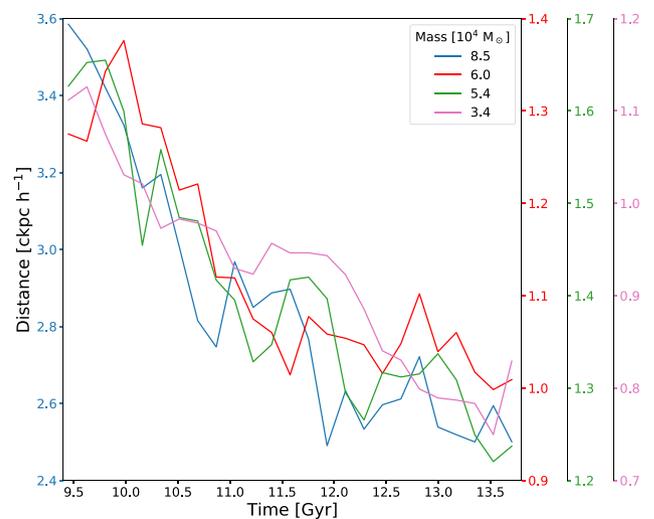
Figure 2. Time evolution of the radial distance of IMBHs in Set 1, with respect to the centre of the MW. Distances are binned, with 25 bins and a mean bin size of ~23 sub-box snapshots (~ 0.177 Gyr). Four vertical axes are used to show overall trends over different distance ranges. For all four IMBHs, radial distance tends to decrease with increasing time.
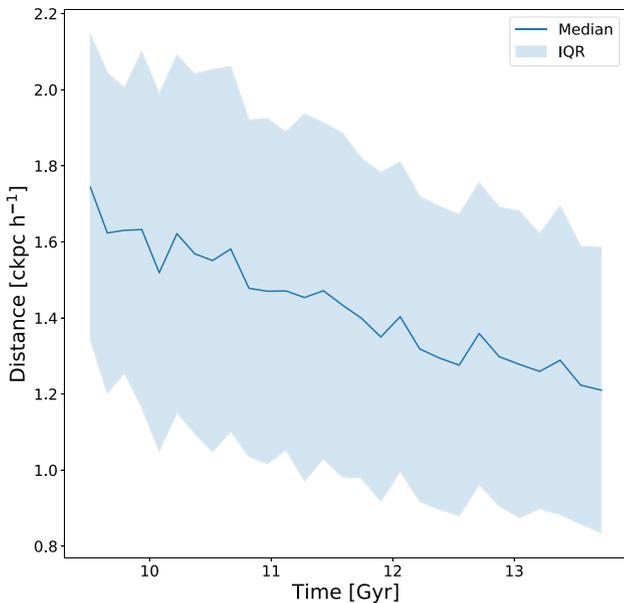
Figure 3. Distribution of radial distances from the centre of the MW for IMBHs in Set 2, with respect to time. These IMBHs originate in a dwarf galaxy, within 0.05 ckpc of the centre. Both the median distance and the interquartile range (IQR) are shown. As time progresses, the radial distance tends to decrease.
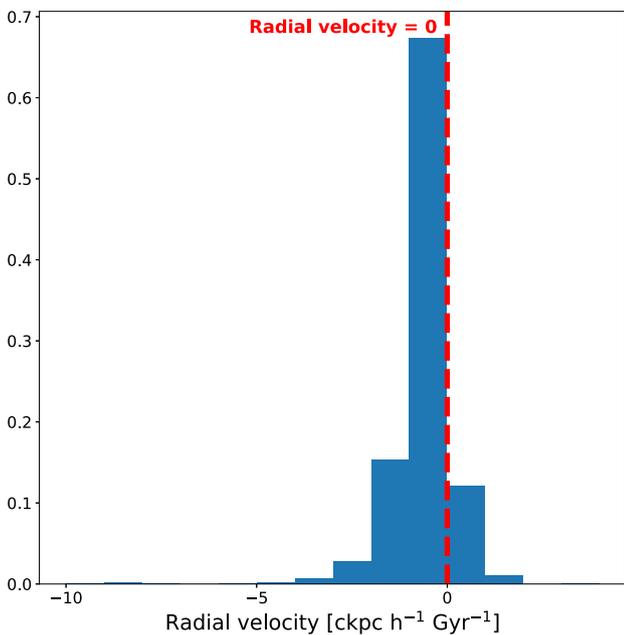
Figure 4. Long-term radial velocity distribution for IMBHs in Set 4 relative to the position of the MW centre. These IMBHs originate outside the MW but are later captured, and they are subject to the restrictions described in Section 3.2. The radial velocities come from a linear fit to the radial distance versus time data of each IMBH, calculated over eight snapshots spanning ~ 3.0 Gyr. The vertical line indicates zero radial velocity. We find that ~ 86.6 per cent of the IMBHs have negative radial velocity, i.e. they are sinking.

the presence of $\sim 25\,000$ stellar mass black holes ($M_\bullet \gtrsim 30\,\mathrm{M}_\odot$) surrounding the central SMBH of the MW.

3.2 Radial velocity and preferred location of IMBHs

In the paragraphs above we showed that, on average, IMBHs are moving to smaller radii with time. To further study their long-term behaviour, we calculated the secular radial velocity of a subset of the IMBHs in Set 3, i.e. our most extensive collection. In particular, we found the distance from the MW centre for each IMBH at snapshots 81–84 ($\sim 10.8 - 11.3$ Gyr) and 96–99 ($\sim 13.3 - 13.8$ Gyr) of the main simulation. We chose this ~ 3.0 Gyr time period as a balance between avoiding small-scale variations while also refraining from assuming constant velocity on large time-scales.

We then calculated the best linear fit to this radial distance versus time data for each IMBH. The slope gives the long-term radial velocity of the IMBH relative to the MW centre, and the value of the line at ~ 13.8 Gyr gives the distance from the MW centre at $z = 0$.

To avoid any dynamic instability from IMBHs that just merged with the MW, we excluded any IMBHs that are not present in the MW for at least two snapshots prior to the studied time period (snapshots 79 and 80). We also excluded any IMBHs that are within $1\,\mathrm{ckpc\,h^{-1}}$ of the MW centre in snapshots 81–84, as well as any IMBHs whose estimated radial velocity changes by $1\,\mathrm{ckpc\,h^{-1}\,Gyr^{-1}}$ or more when calculated using snapshots 81–84 and 88–91 (rather than 81–84 and 96–99). This helps ensure that we are not considering IMBHs that reach the central region of the MW before or near the beginning of the studied time period. These IMBHs would likely stay near the centre for the entire time period, causing the radial velocity to be underestimated. Note that a few other IMBHs were excluded because, while they were present in the MW in snapshots 79 and 80, and still in the MW at snapshot 99, they were not classified as part of the MW in one or more of the other studied snapshots. There are 953 IMBHs that meet all of these requirements. We call this group Set 4 (see Table 1).

Fig. 4 shows a histogram of radial velocities. The vertical values are normalized such that their integral is unity (from now on we will refer to this simply as a normalized histogram). We found that 825 IMBHs (~ 86.6 per cent of Set 4) have negative radial velocity, with 640 (~ 67.2 per cent) between -1 and $0\,\mathrm{ckpc\,h^{-1}\,Gyr^{-1}}$. We call the group of 825 sinking IMBHs Set 5 (see Table 1). The median radial velocity of this set is $\sim -0.44\,\mathrm{ckpc\,h^{-1}\,Gyr^{-1}}$. These results suggest that most captured IMBHs in the MW sink towards the galactic centre.

Fig. 5 shows a normalized histogram of radial distances at $z = 0$. We found that 41 IMBHs (~ 4.3 per cent of Set 4) reach the central volume of the MW, defined as the innermost sphere with a radius of $1\,\mathrm{ckpc\,h^{-1}}$. Recall that none of the IMBHs in Set 4 were in this region just ~ 2.5 Gyr earlier, at snapshot 84.

The resulting IMBH number density within the central $1\,\mathrm{ckpc\,h^{-1}}$ is ~ 1.6 times the value found within the central $2\,\mathrm{ckpc\,h^{-1}}$. As shown in the histogram, distance ranges past $2\,\mathrm{ckpc\,h^{-1}}$ contain much smaller numbers of IMBHs. Thus, our simulations suggest that the central $\sim 1\,\mathrm{ckpc\,h^{-1}}$ of the Galaxy holds the highest density of IMBHs.

To conclude, it is worth noting that, as our IMBHs in Sets 1 and 2 are chosen to be strongly bound to the host dwarf galaxy, none of them are ejected during the merging process with the MW analogue. Interestingly, we computed that ~ 7.5 per cent of the IMBHs in Set 2 have a positive total energy with respect to the MW in snapshot 72 (the first snapshot after the merging event). None the less, these IMBH proxies are still counted as part of the MW until the very end
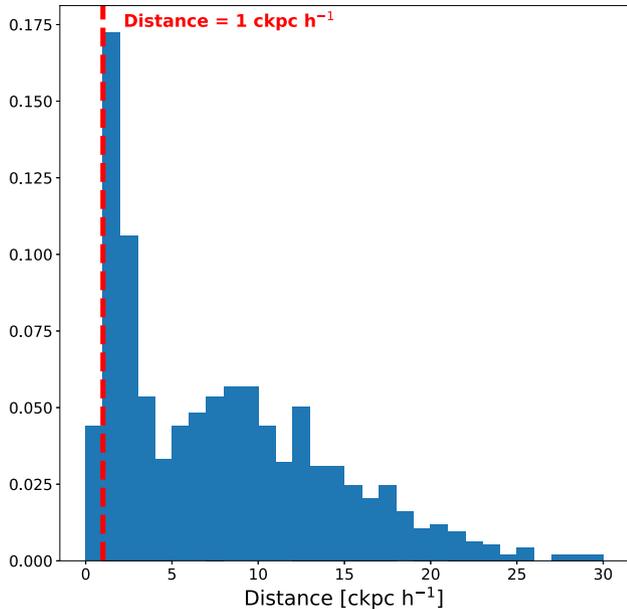
Figure 5. Distance distribution with respect to the MW centre for IMBHs in Set 4. The distances are computed at $z = 0$, using the linear fits to the radial distance versus time data of each IMBH. The distance is cut at 30 ckpc h^{-1} for a better visualization, with a vertical line indicating a distance of 1 ckpc h^{-1}. We find that ~ 4.3 per cent of the IMBHs fall within the innermost 1 ckpc h^{-1}, suggesting that the highest density of IMBHs lies in the central region of the Galaxy.

of the simulation, hence they are never practically ejected from the gravitational system.

4 KINEMATICS AND DYNAMICS OF IMBHS IN THE MW

In this section, we study the kinematics of IMBHs in the MW, with a particular focus on the distribution of their 3D velocities with respect to the centre of the MW and with respect to the surrounding gas.

4.1 Radial distribution of 3D velocities

To study the radial velocity distribution, we used Set 3, our most extensive IMBH catalogue, and worked in snapshot 99 ($z \approx 0$). For each IMBH, we calculated the distance from the MW centre and the magnitude of the velocity vector relative to the MW centre. We then sorted the velocity magnitudes into groups by their corresponding radial distances and found a Gaussian fit for the velocity distribution of each group. Fig. 6 shows normalized histograms (with 16 bins each) and Gaussian fits for groups with corresponding radial distances up to 30 ckpc h^{-1}. Table 2 gives the statistical descriptors of these Gaussian fits.

Next, for every IMBH, we calculated the velocity vector relative to each of the four closest gas particles. We then calculated the mean of the magnitudes of the four velocity vectors for each IMBH and, as before, sorted the mean velocity magnitudes into groups based on radial distance from the MW centre. Fig. 7 shows normalized histograms (with 16 bins) for each group up to 30 ckpc h^{-1}. Also included are skewed normal fits for the velocity distribution of each group. Table 2 gives the statistical descriptors of these skewed fits. In implementing the skewed normal distribution, we used the definition provided by Azzalini & Capitanio (2009).
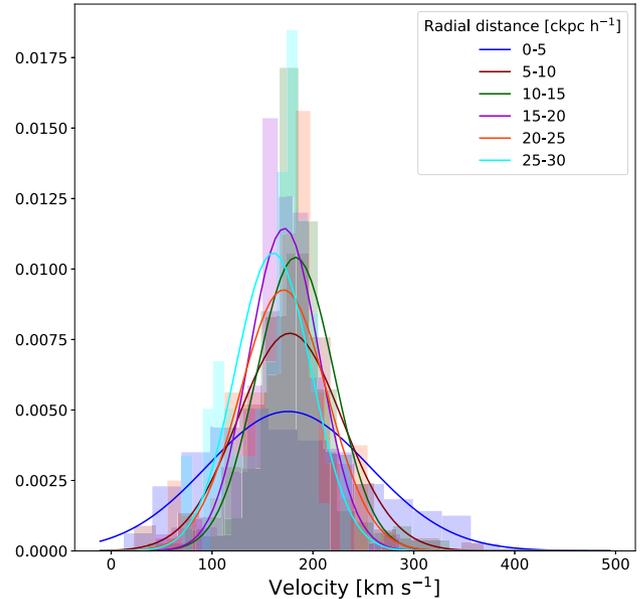
Figure 6. Distribution of 3D velocities for IMBHs in Set 3 with respect to the MW centre, calculated at $z \approx 0$. These IMBHs originate outside the MW and are later captured. Radial distributions are divided into groups of 5 ckpc h^{-1} each. Gaussian fits to each velocity distribution are provided.

We recognize that the histograms in Fig. 6 are not necessarily Gaussian, but we use this distribution as the simplest one to obtain some statistical information on the mean and variance of the histograms. With a Gaussian fit we intend to provide a simple description of the data, not to infer any physical interpretation on its origin. The Gaussian fits in Fig. 6 are also used to highlight the strong contrast with the distributions of velocities relative to the local gas (Fig. 7), which are, instead, strongly non-Gaussian (except the radial bin $0 - 5$ ckpc h^{-1}) and fitted with a skewed function.

Fig. 6 shows that typical velocities of IMBHs with respect to the centre of the MW are ~ 180 km s^{-1}, with larger variance as the radial distance decreases. In particular, we note that the variance is a factor ~ 2 larger in the innermost radial bin than in the outermost bin. This may be due to a larger number of IMBHs in the inner bins, but a higher stellar velocity variance with decreasing galactocentric distance is also observed and predicted by models (Battaglia et al. 2005; Dehnen, McLaughlin & Sachania 2006; Brown et al. 2010).

Fig. 7 shows that velocity magnitudes relative to the local gas are significantly lower, typically ~ 88 km s^{-1} (for radial distances $\gtrsim 5$ ckpc h^{-1}), and the distribution is highly skewed towards high values. The distribution of IMBH velocities with respect to the local gas was obtained because it is relevant for the calculation of accretion rates on to wandering IMBHs in the MW. In fact, classical Bondi accretion calculations (Bondi 1952) rely on the velocity of the wandering object with respect to the local gas frame. More details on this issue are discussed in Section 5.

To explain the high velocity of the $0 - 5$ ckpc h^{-1} range in Fig. 7, we found the radial distance and velocity magnitude relative to the MW centre for each gas particle in the MW. We then sorted the velocity versus distance data into 1 ckpc h^{-1} bins and found the median velocity of each group. The results, shown in Fig. 8, suggest that the gas velocity in the central 5 ckpc h^{-1} of the MW is significantly high, and explained by the presence of a $\sim 9 \times 10^7$ M$_\odot$ SMBH at the centre of the MW analogue. Fig. 8 also shows the orbital velocity around a typical $\sim 10^8$ M$_\odot$ SMBH at radial distances

Table 2. Statistical descriptors of the velocity distribution of IMBHs with respect to the centre of the MW and to the local gas. The data relative to the MW centre are fitted with a Gaussian probability distribution function. The data relative to the local gas are fitted with a skewed probability distribution. All values are rounded to two decimals.

Distance range (ckpc h^{-1})	MW centre		Local gas		
	Mean (km s^{-1})	Std. deviation (km s^{-1})	Mean (km s^{-1})	Std. deviation (km s^{-1})	Skewness parameter
0 − 5	175.46	80.64	384.25	135.11	0.69
5 − 10	177.15	51.66	114.22	85.70	18.30
10 − 15	182.73	38.31	77.42	77.47	38.22
15 − 20	171.58	34.86	71.80	63.34	16.76
20 − 25	170.90	43.07	90.17	82.88	75.03
25 − 30	160.69	37.74	92.11	84.62	6839254.74
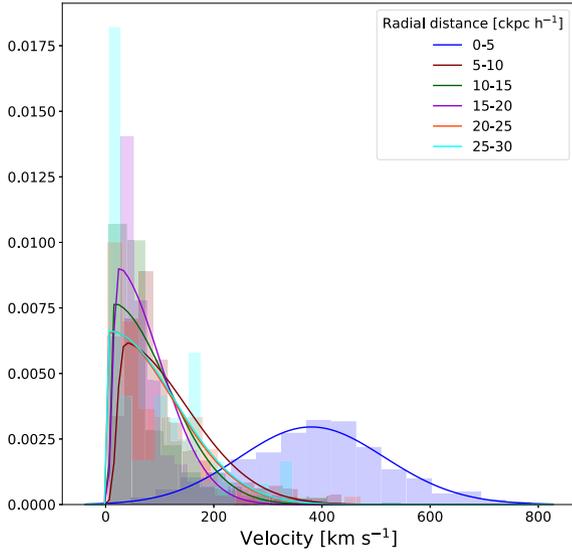
Figure 7. As in Fig. 6, but with velocities calculated with respect to the local gas frame. Skewed Gaussian fits are also provided. This distribution is useful for calculating the accretion rates on to IMBHs wandering in the MW.

Figure 9. Sinking velocity versus radial distance relative to the MW centre for IMBHs in Set 5 with radial distances less than 30 ckpc h^{-1}. These are captured IMBHs with negative radial velocity, subject to certain conditions described in Section 3.2. The data are shown as a scatter plot, with binned values and the empirical fit also provided. The fact that sinking velocities tend to get smaller with decreasing distance from the galactic centre indicates that IMBH orbits circularize as they sink farther into the MW.

of 100 AU and 0.1 pc, as well as the rotational velocity of stars in the MW up to 25 kpc from Li (2016).

4.2 Orbital circularization

We now turn our attention to sinking IMBHs. For each IMBH in Set 5, we found the value of the best-fitting line from Section 3.2 at ∼ 12.3 Gyr (the mean of the eight times at which radial distance was measured). This gave us an estimate for the distance from the MW centre. We then considered sinking (radial) velocity versus radial distance for the 808 sinking IMBHs with radial distances less than 30 ckpc h^{-1}. Fig. 9 shows a scatter plot of the data, as well as the mean sinking velocity over 1 ckpc h^{-1} bins (darker blue line). We found the binned data to be well-fitted by an empirical curve of the form:

$$V = kR^p, \tag{1}$$

where V and R are the sinking velocity in ckpc h^{-1} Gyr^{-1} and radial distance in ckpc h^{-1}, respectively, both functions of the simulation

Figure 8. Median gas velocity magnitude (relative to MW centre) versus radial distance. The two horizontal, dashed lines represent the orbital velocity around a 10^8 M$_\odot$ SMBH, at 100 AU and at 0.1 pc, for reference. Also shown is the rotational velocity of the MW up to 25 kpc (Li 2016).
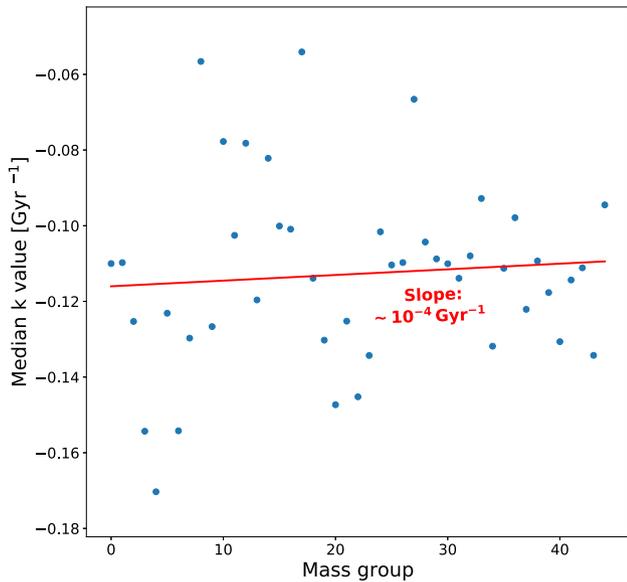
Figure 10. Median k value versus group number. Here, k is the constant of proportionality in the empirically derived relation $V = kR^p$ between sinking velocity and radial distance. IMBHs in Set 5 with radial distances less than $30\,\mathrm{ckpc}\,h^{-1}$ are divided by mass into 45 groups, where the group number increases with increasing mass. The best-fitting line to this data is shown, and the very small slope indicates that sinking velocity does not depend on black hole mass.

time t in Gyr. We found $k \approx -0.10846\,\mathrm{Gyr}^{-1}$ and $p \approx 0.83472$. The results of the regression are added to Fig. 9 as a red line.

The fact that the magnitude of the radial velocity $V(t)$ declines as an IMBH approaches the centre matches our expectation that the orbits of the IMBHs circularize as they sink farther into the MW (for a semi-analytical treatment of this effect, see e.g. Bonetti et al. 2020). Solving the ordinary differential equation in equation (1), with integration constant $R(t = 0) = R_0$, we find:

$$R(t) = \left[R_0^{(1-p)} + k\,t\,(1-p) \right]^{\frac{1}{1-p}}. \tag{2}$$

We divided this IMBH data set into 45 mass bins and calculated the median value of $k = V/R^p$ (where we keep $p \approx 0.83472$) for each group. We plotted the median k values versus group number, as shown in Fig. 10, and obtained a best-fitting line with a slope of $\sim 1.4951 \times 10^{-4}\,\mathrm{Gyr}^{-1}$, indicating virtually no dependence on mass. In other words, the sinking velocity does not depend on the mass of the IMBH. This result is interesting because one would naively expect heavier black holes to sink faster. In reality, IMBHs sink inefficiently towards the centre, especially when wandering inside clumpier galaxies. For example, Ma et al. (2021) have recently suggested that in high-z clumpy galaxies, black holes less massive than $10^8\,\mathrm{M}_\odot$ (a limit that includes our entire mass range) migrate inefficiently towards the centre, with velocity magnitudes changing erratically and a much slower deceleration.

The empirical model in equation (1) is useful to determine general trends in the data, but it does not provide any information regarding the forces acting to reduce the radial velocity as the IMBH sinks. Below, we develop a toy model to study the circularization effect and gain useful insights into the processes that lead to it.

We assume for simplicity a linear drag force of the form $-bV$ (see e.g. Chandrasekhar 1943) and a gravitational force $GM_\bullet M(R)/R^2$, where $M_\bullet$ is the mass of the IMBH, $M(R)$ is the mass of the MW

contained within the radius R, and b is the drag force constant, with dimensions equal to a mass over a time. Note that a linear drag force is appropriate when the IMBH is moving through a non-turbulent medium at relatively low (radial) speed. In addition, we assume an MW with a constant mass density ρ. We let $t = 0$ mark the time at which the IMBH entered the MW, and assume for simplicity $V(t = 0) = 0$. We also let $R(t = 0) = R_0$, and find a solution of the initial value problem of the form:

$$R(t) = \frac{R_0}{2\Phi} \left[(1 + \Phi)\, e^{-\frac{b}{2M}(1-\Phi)t} - (1 - \Phi)\, e^{-\frac{b}{2M}(1+\Phi)t} \right], \tag{3}$$

where:

$$\Phi = \sqrt{1 - \frac{16\pi G \rho M^2}{3b^2}} \tag{4}$$

is a dimension-less parameter that controls the rate at which the radius decreases.

Next, we found best-fitting curves of the forms in equations (2) and (3) for the radial distance versus time data of each IMBH in Set 1. Here, t represents the time since the dwarf galaxy hosting these four IMBHs merged with the MW (at snapshot 71, or ~ 9.2 Gyr). The results are shown in Fig. 11, with the fit parameters for the physical model listed in Table 3. Visually, both the empirical and physical models are successful in reproducing the decreasing distance of the IMBHs with increasing time. We also show in Fig. 12 the residuals between the physical and empirical models and the simulation data. These small differences support the conclusion that our models are good fits for the data.

We note that the values of the parameters $b/2M$ are consistent with each other, and the parameter of linear drag, b, is proportional to the mass of the perturber, M (Binney & Tremaine 1987). Interestingly, the values of the initial distances, R_0 are similar to each other, except for the heaviest IMBH which is approximately the double. Similar initial distances are expected, because all the IMBHs are originating from the same dwarf galaxy, which merges with the MW. We investigated this issue further, and found that the dwarf galaxy merged with the MW at snapshot 71, at which point the heaviest IMBH becomes classified as a particle belonging to the MW. However, the three lighter IMBHs become part of the MW only at the following snapshot 72. We hypothesize that some complex encounter dynamics may have influenced the association of the heaviest IMBH earlier than the others, so that its initial radius is also larger.

The physical model described by equation (3) allowed us to quantify some relevant physical parameters. First, we used equation (4) and Table 3 to calculate ρ from the fit parameters for each IMBH in Set 1. We found a mean density of $\sim 2.21 \times 10^{-4}\,\mathrm{M}_\odot\,\mathrm{pc}^{-3}$, with a standard deviation of $\sim 2.23 \times 10^{-5}\,\mathrm{M}_\odot\,\mathrm{pc}^{-3}$. For comparison, we calculated the average density of the MW analogue within the half-mass radius, in each snapshot from 71 to 99. The mean density over these snapshots was $5.05 \times 10^{-5}\,\mathrm{M}_\odot\,\mathrm{pc}^{-3}$. Note that the half-mass radius of the MW is $\sim 38.4\,\mathrm{ckpc}\,h^{-1}$, much larger than the radial distances of the IMBHs in Set 4, so it makes sense that the average density calculated using this half-mass radius would be lower than the estimate from our physical model. Therefore we conclude that our model provides a reasonable density estimate.

We also estimated the time needed for an IMBH to reach a radial distance of $1\,\mathrm{ckpc}\,h^{-1}$, using equation (3) and the mean values of R_0, Φ, and $b/2M$ from Table 3, finding a sinking time-scale of ~ 8.3 Gyr.

We note that in our analysis we focused on IMBHs with $v < 0$, i.e. on sinking particles. Of course, as the drag force would work to oppose the velocity independently of the direction of the velocity vector, our model would apply also for particles with $v > 0$. In
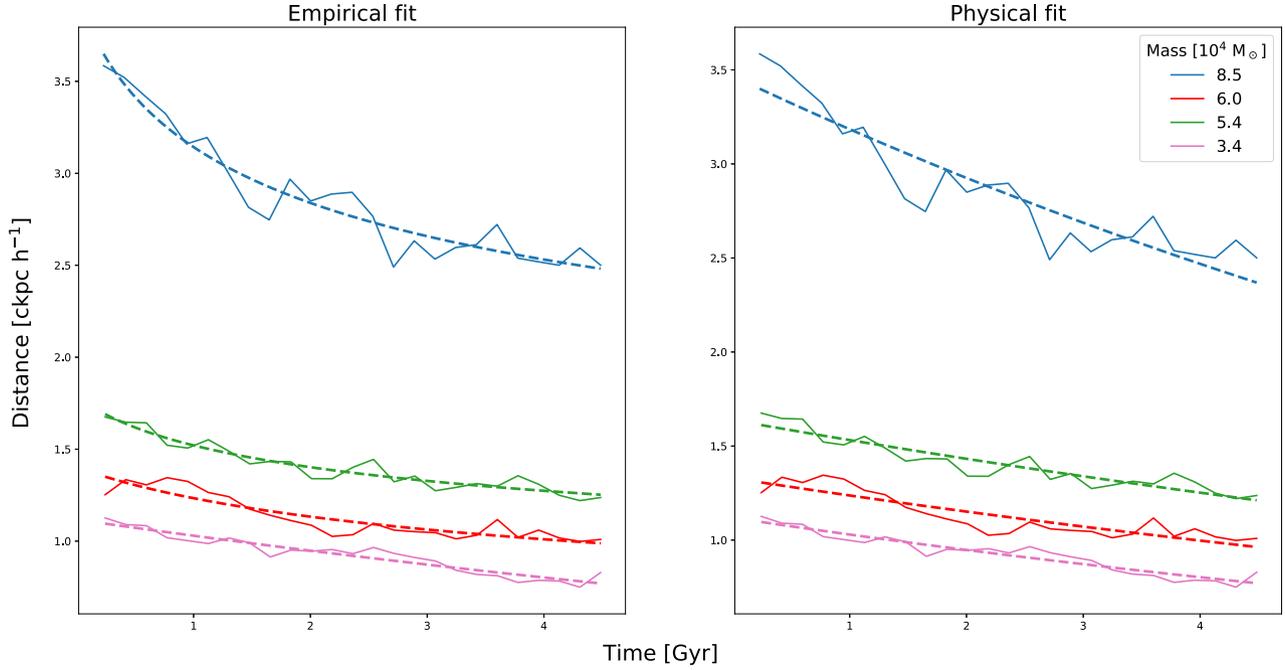
Figure 11. Radial distance versus time for IMBHs in Set 1 (our smallest set, with the highest time resolution data). Fits from the empirical (equation 2) and physical (equation 3) models are shown as dashed lines. Visually, both models are good fits for the data.

Table 3. Parameters for the physical model fit to the radial distance versus time data for IMBHs in Set 1. Rounded to three decimals.

Black hole mass (10^4 $M_\odot$)	R_0 (ckpc h^{-1})	Φ	$b/2M$ (Gyr^{-1})
8.5	3.461	0.997	27.543
6.0	1.327	0.997	27.066
5.4	1.636	0.998	27.114
3.4	1.117	0.997	27.043

Figure 12. Difference between the empirical (dotted line) and physical (solid line) best-fitting curves and the simulation data for each IMBH in Set 1. The small residuals indicate that our physical and empirical models fit the data well.

fact, for IMBHs with positive radial velocities, their magnitudes are lower at smaller galactocentric distances. In Fig. 9 we limit our analysis to sinking IMBHs because: (i) we are mostly interested in particles that, in the long term, are approaching the centre, because of the implications for the possibility of observing them, and (ii) they represent the majority of IMBHs studied.

The study of the effect of dynamical friction in the sinking (or not) of central black holes in merging galaxies is, of course, not new. Early works (e.g. Governato, Colpi & Maraschi 1994; Mayer et al. 2007) already showed the importance of dynamical friction from gas which leads central SMBHs in merging galaxies to approach each other, over sinking time-scales of several Gyrs. More recent works have stressed the challenges in approaching distances shorter than ~100 pc in minor mergers (see e.g. Dosopoulou & Antonini 2017), the dependence on the mass ratio of the merging galaxies (see e.g. Tremmel et al. 2018), and the importance of the stellar component in the dynamical process, which can be dominant for IMBHs especially at high-z (see e.g. Pfister et al. 2019).

5 DISCUSSION AND CONCLUSIONS

In this study, we used the TNG50 cosmological simulation from the IllustrisTNG project to study the kinematics and dynamics of putative IMBHs wandering in the MW, as a result of their capture during mergers with dwarf galaxies. Some of the most relevant results are the following:

(i) A fraction ~ 86.6 per cent of captured IMBHs in the MW are sinking;

(ii) The highest density of IMBHs occurs in the central 1 ckpc h^{-1} region of the Galaxy, with a number density ~1.6 times higher than in the central 2 ckpc h^{-1} region;

(iii) The 3D velocities of IMBHs relative the MW centre are $\gtrsim$ 2 times larger than those relative to the local gas. Typical velocities with respect to the local gas are ~ 88 km s^{-1};
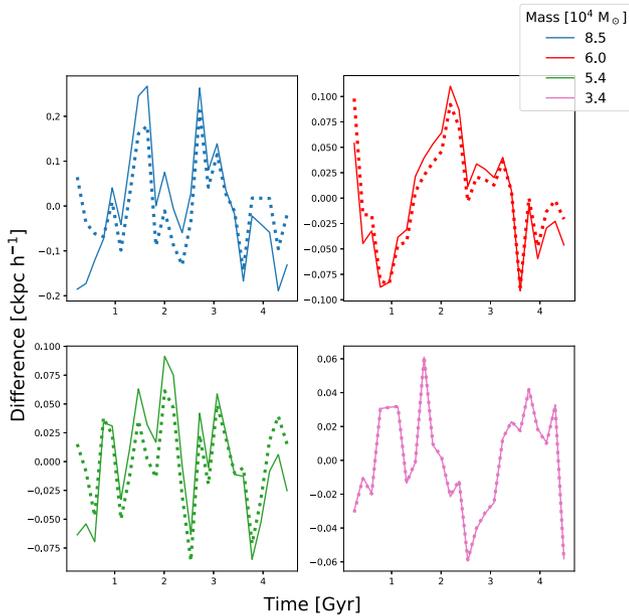
(iv) Sinking velocities of IMBHs decline with decreasing radial distance, with a circularization of the orbits possibly due to drag effects.

These results will influence future studies of IMBHs wandering not only in the MW, but also in other galaxies. By locating the volume of the Galaxy containing the highest density of IMBHs, we provide guidance for observational efforts to detect these objects. Several studies have started to investigate the putative population of massive and supermassive wandering black holes in galaxies (see e.g. Bellovary et al. 2010; Ricarte et al. 2021a,b). In particular, Bellovary et al. (2010) predict that the MW should host 5–15 IMBHs within its halo, while more recent studies (Ricarte et al. 2021a) provide higher estimates.

Our results concerning velocity distributions relative to the galactic centre and surrounding gas allow calculations of Bondi (Bondi 1952) or Bondi-like accretion rates for IMBHs. Due to the low-density, non-central environments that should host these IMBHs, the appropriate mode to describe their accretion is an advection-dominated accretion flow, or ADAF (Narayan & Yi 1994, 1995; Abramowicz et al. 1995; Narayan & McClintock 2008; Yuan & Narayan 2014), possibly modified to take into account the effects of convection and outflows (Igumenshchev, Narayan & Abramowicz 2003; Proga & Begelman 2003). Note that already Bellovary et al. (2010) predicted that off-nuclear black holes could be detected as ultraluminous X-ray sources.

Finally, the spatial and velocity distributions of these objects can inform predictions of gravitational wave events generated by merging IMBHs in the MW. It is possible that the current and future gravitational wave detectors such as LIGO, Virgo, KAGRA, and the Laser Interferometer Space Antenna (LISA; Amaro-Seoane et al. 2017) could detect these merging events in the MW or nearby major galaxies (see e.g. Pacucci & Loeb 2020). For example, Fragione, Ginsburg & Kocsis (2018) predict that up to ∼1000 IMBHs, with masses in the range $10^3 - 10^4\,\mathrm{M}_\odot$ in their model, could be wandering within ∼ 1 kpc of the Galactic centre, generating signals detectable in the gravitational waves domain.

Of course, our findings come with several caveats. While we study over 2000 IMBHs, several hundred of which came from the same dwarf galaxy, we are not suggesting that the MW, or dwarfs merging with the MW, contain this many actual IMBHs. Rather, our study provides a statistical sampling of the location and velocity distribution of IMBHs in the MW, without offering any insights on their actual number.

As explained in Section 2.2, the IMBHs used are proxies, i.e. stellar objects in the correct mass range. Their gravitational effect on the environment should be the same, as noted also by, e.g. Mistani et al. (2016), where the authors used the same technique for globular clusters instead of IMBHs. Nevertheless, this is a point worth remembering when considering our results. One effect of using star clusters as proxies, also discussed in Section 2.2, is that they only cover a fraction of the typical mass range of IMBHs. Additionally, cluster objects are subject to some mass-loss through evaporation. In our simulations, IMBH proxies have a median mass-loss of ∼ 3.6 per cent over the time frame investigated (snapshots 81–99), which is too small to affect our conclusions. Finally, we note that our kinematic and dynamical analyses are constrained by a time resolution of ∼ 0.14 Gyr in the main simulation, and ∼ 0.004 Gyr in sub-box 2.

In summary, this study is an important first step in investigating the properties of captured IMBHs in the MW. Despite large unknowns in their properties and regarding their very existence in the MW, efforts to detect them are underway, and are crucial to understand the last unknown black hole population in our Galaxy.

DATA AVAILABILITY

The data underlying this article are available on the website of the IllustrisTNG project, as described in Nelson et al. (2019a). The codes used to analyse the data will be shared on reasonable request to the corresponding author.

REFERENCES

Abramowicz M. A., Chen X., Kato S., Lasota J.-P, Regev O., 1995, ApJ, 438, L37

Alexander T., Natarajan P., 2014, Science, 345, 1330

Amaro-Seoane P. et al., 2017, preprint (arXiv:1702.00786)

Azzalini A., Capitanio A., 2009, preprint (arXiv:0911.2093)

Baldassare V. F., Reines A. E., Gallo E., Greene J. E., 2015, ApJ, 809, L14

Baldassare V. F., Reines A. E., Gallo E., Greene J. E., 2017, ApJ, 850, 196

Baldassare V. F., Dickey C., Geha M., Reines A. E., 2020, ApJ, 898, L3

Battaglia G. et al., 2005, MNRAS, 364, 433

Bellovary J. M., Governato F., Quinn T. R., Wadsley J., Shen S., Volonteri M., 2010, ApJ, 721, L148

Binney J., Tremaine S., 1987, Galactic Dynamics. Princeton Univ. Press, Princeton

Bondi H., 1952, MNRAS, 112, 195

Bonetti M., Bortolas E., Lupi A., Dotti M., Raimundo S. I., 2020, MNRAS, 494, 3053

Brown W. R., Geller M. J., Kenyon S. J., Diaferio A., 2010, AJ, 139, 59

Chandrasekhar S., 1943, ApJ, 97, 255

Dehnen W., McLaughlin D. E., Sachania J., 2006, MNRAS, 369, 1688

Dosopoulou F., Antonini F., 2017, ApJ, 840, 31

Dullo B. T., Gil de Paz A., Knapen J. H., 2021, ApJ, 908, 134

Elbert O. D., Bullock J. S., Kaplinghat M., 2018, MNRAS, 473, 1186

Engler C. et al., 2021, MNRAS, 507, 4211

Event Horizon Telescope Collaboration, 2019, ApJ, 875, L1

Ferrarese L., Merritt D., 2000, ApJ, 539, L9

Fragione G., Ginsburg I., Kocsis B., 2018, ApJ, 856, 92

Gebhardt K. et al., 2000, ApJ, 539, L13

Genzel R., Eisenhauer F., Gillessen S., 2010, Rev. Mod. Phys., 82, 3121
Ghez A. M. et al., 2008, ApJ, 689, 1044
González J. A., Guzmán F. S., 2018, Phys. Rev. D, 97, 063001
González E., Kremer K., Chatterjee S., Fragione G., Rodriguez C. L., Weatherford N. C., Ye C. S., Rasio F. A., 2021, ApJ, 908, L29
Governato F., Colpi M., Maraschi L., 1994, MNRAS, 271, 317
Greene J. E., Strader J., Ho L. C., 2020, ARA&A, 58, 257
Greene J. E. et al., 2021, ApJ, 917, 17
Gürkan M. A., Freitag M., Rasio F. A., 2004, ApJ, 604, 632
Igumenshchev I. V., Narayan R., Abramowicz M. A., 2003, ApJ, 592, 1042
Kormendy J., Ho L. C., 2013, ARA&A, 51, 511
Kruijssen J. M. D. et al., 2020, MNRAS, 498, 2472
Li E., 2016, preprint (arXiv:1612.07781)
Ma L., Hopkins P. F., Ma X., Anglés-Alcázar D., Faucher-Giguère C.-A., Kelley L. Z., 2021, MNRAS, 508, 1973
Marinacci F. et al., 2018, MNRAS, 480, 5113
Mayer L., Kazantzidis S., Madau P., Colpi M., Quinn T., Wadsley J., 2007, Science, 316, 1874
Miralda-Escudé J., Gould A., 2000, ApJ, 545, 847
Mistani P. A. et al., 2016, MNRAS, 455, 2323
Naiman J. P. et al., 2018, MNRAS, 477, 1206
Narayan R., McClintock J. E., 2008, New Astron. Rev., 51, 733
Narayan R., Yi I., 1994, ApJ, 428, L13
Narayan R., Yi I., 1995, ApJ, 452, 710
Natarajan P., 2021, MNRAS, 501, 1413
Nelson D. et al., 2018, MNRAS, 475, 624
Nelson D. et al., 2019a, Comput. Astrophys. Cosmol., 6, 2
Nelson D. et al., 2019b, MNRAS, 490, 3234
Nguyen D. D. et al., 2019, ApJ, 872, 104
Oke J. B., 1977, ApJ, 217, 181
Pacucci F., Loeb A., 2020, ApJ, 895, 95
Pacucci F., Loeb A., Mezcua M., Martín-Navarro I., 2018, ApJ, 864, L6
Pacucci F., Mezcua M., Regan J. A., 2021, ApJ, 920, 134
Pfister H., Volonteri M., Dubois Y., Dotti M., Colpi M., 2019, MNRAS, 486, 101
Pillepich A. et al., 2018a, MNRAS, 473, 4077
Pillepich A. et al., 2018b, MNRAS, 475, 648
Pillepich A. et al., 2019, MNRAS, 490, 3196
Pillepich A., Nelson D., Truong N., Weinberger R., Martin-Navarro I., Springel V., Faber S. M., Hernquist L., 2021, MNRAS, 508, 4667
Planck Collaboration VI, 2020, A&A, 641, A6
Portegies Zwart S. F., McMillan S. L. W., 2002, ApJ, 576, 899
Proga D., Begelman M. C., 2003, ApJ, 592, 767
Ricarte A., Tremmel M., Natarajan P., Zimmer C., Quinn T., 2021a, MNRAS, 503, 6098
Ricarte A., Tremmel M., Natarajan P., Quinn T., 2021b, ApJ, 916, L18
Ryu T., Tanaka T. L., Perna R., Haiman Z., 2016, MNRAS, 460, 4122
Schleicher D. R. G., Palla F., Ferrara A., Galli D., Latif M., 2013, A&A, 558, A59
Shi Y., Grudić M. Y., Hopkins P. F., 2021, MNRAS, 505, 2753
Springel V., 2010, MNRAS, 401, 791
Springel V. et al., 2018, MNRAS, 475, 676
Thompson T. A. et al., 2019, Science, 366, 637
Tremmel M., Governato F., Volonteri M., Quinn T. R., Pontzen A., 2018, MNRAS, 475, 4967
Volonteri M., Begelman M. C., 2010, MNRAS, 409, 1022
Wang F. et al., 2021, ApJ, 907, L1
Yuan F., Narayan R., 2014, ARA&A, 52, 529

This paper has been typeset from a TeX/LaTeX file prepared by the author.